Version of Record at: https://doi.org/10.1029/2024JC021299

AGU ADVANCING EARTH AND SPACE SCIENCES

JGR Oceans

RESEARCH ARTICLE
10.1029/2024JC021299

Hypoxia Triggered by Expanding River Plume on the East China Sea Inner Shelf During Flood Years

Dewang Li[1,2,3], Jianfang Chen[1,4], Bin Wang[1,2], Haiyan Jin[1,4], Lu Shou[1,3], Hua Lin[1], Yanyi Miao[1,5], Qianwen Sun[1,6], Zhibing Jiang[1], Qicheng Meng[4], Jiangning Zeng[1,4], Feng Zhou[3,4], and Wei-Jun Cai[7]

[1]Key Laboratory of Marine Ecosystem Dynamics, Second Institute of Oceanography, Ministry of Natural Resources, Hangzhou, China, [2]Donghai Laboratory, Zhoushan, China, [3]Observation and Research Station of Yangtze River Delta Marine Ecosystems, Ministry of Natural Resources, Zhoushan, China, [4]State Key Laboratory of Satellite Ocean Environment Dynamics, Second Institute of Oceanography, Ministry of Natural Resources, Hangzhou, China, [5]School of Oceanography, Shanghai Jiao Tong University, Shanghai, China, [6]Ocean College, Zhejiang University, Zhoushan, China, [7]School of Marine Science and Policy, University of Delaware, Newark, DE, USA

Key Points:

- We observed a maximum hypoxia area of ~11,600 km^2, and a minimum dissolved oxygen of 21 μmol L^{-1} during the flood period in 2020
- Significant nitrate removal and surface Chlorophyll *a* exceeding 29 μg L^{-1} suggested intense biological production during the flood period
- The expansion of high-Chl *a* plume area during flood periods surpasses that of non-flood periods, contributing to hypoxia area increase

Supporting Information:

Supporting Information may be found in the online version of this article.

Correspondence to:

J. F. Chen,
jfchen@sio.org.cn

Citation:

Li, D. W., Chen, J. F., Wang, B., Jin, H. Y., Shou, L., Lin, H., et al. (2024). Hypoxia triggered by expanding river plume on the East China Sea inner shelf during flood years. *Journal of Geophysical Research: Oceans*, *129*, e2024JC021299. https://doi.org/10.1029/2024JC021299

Received 4 MAY 2024
Accepted 2 JUL 2024

Author Contributions:

Conceptualization: Dewang Li, Jianfang Chen
Data curation: Dewang Li, Bin Wang, Lu Shou, Yanyi Miao, Qianwen Sun, Zhibing Jiang, Qicheng Meng, Jiangning Zeng, Feng Zhou
Formal analysis: Dewang Li, Jianfang Chen, Bin Wang, Qicheng Meng, Wei-Jun Cai
Funding acquisition: Jianfang Chen, Haiyan Jin, Jiangning Zeng
Investigation: Dewang Li, Lu Shou, Hua Lin, Yanyi Miao, Qianwen Sun, Zhibing Jiang
Project administration: Jianfang Chen
Validation: Dewang Li, Jianfang Chen, Bin Wang, Wei-Jun Cai
Writing – original draft: Dewang Li
Writing – review & editing: Dewang Li, Jianfang Chen, Bin Wang, Haiyan Jin,

Abstract The frequency of riverine floods is predicted to increase in East Asia. However, the response of coastal hypoxia (<63 μmol L^{-1}) to floods has not been well understood. In the summer of 2020, characterized by one of the most significant Changjiang water fluxes in three decades, we conducted a cruise during the flood period on the East China Sea inner shelf. Our observations revealed severe bottom hypoxia with a maximum spatial coverage of ~11,600 km^2 and a minimum dissolved oxygen concentration (DO) of 21 μmol L^{-1}. In the surface layer, the relationships between salinity and nitrate, dissolved inorganic carbon (DIC) indicated significant organic matter production, validated by a high-Chlorophyll-*a* (Chl *a*) patch (>5 μg L^{-1}). Furthermore, the significant relationship between apparent oxygen utilization and DIC of deep waters reveals that the organic matter decomposition primarily drove the hypoxia during the flood period. Episodic wind events also influenced bottom DO and DIC, by transporting surface waters to the deep. Multiple-years data set shows that the average Changjiang nitrate flux during flood years is about 1.4 times that during non-flood years. The flood waters mix with estuarine waters, forming the high-nutrient plume waters, which expanded farther offshore during the flood period. While high turbidity remained confined to the inner estuary. Consequently, the high-Chl *a* area significantly expanded, which significantly exacerbated the hypoxia.

Plain Language Summary Coastal waters are severely threatened by hypoxia, which impacts the growth, reproduction, and migration of marine organisms. Nutrient inputs from river basins are one of the major controlling factors of hypoxia in coastal oceans. The frequency and intensity of floods in river basins are projected to increase in the context of global warming in East Asia. However, the relationship between floods and coastal hypoxia is not well documented. The year 2020 witnessed lots of riverine flood events across Asian countries, which provided us with an excellent opportunity to reveal the influences of flood on hypoxia development on the shelf. In 2020, the August nitrate flux of Changjiang was 1.5 times higher compared to that in non-flood years. We observed maximum hypoxic waters covering 11,600 km^2 with a minimum DO of 21 μmol L^{-1} on the East China Sea inner shelf. Historical data showed that the floods led to the expansion of the high-nutrient plume area, resulting in high biological production in the plume, and a nearly doubling of the hypoxia extent in the bottom waters. With the growing risk of intensive floods, hypoxia is likely to aggravate in coastal waters.

1. Introduction

Dissolved oxygen (DO) concentrations have been declining globally in the open ocean and coastal waters in the past several decades (Breitburg et al., 2018; Ito et al., 2017). Coastal hypoxia (<63 μmol L^{-1}) was observed in hundreds of sites worldwide. It affects the growth, reproduction, and migration of eukaryotes (Rabalais et al., 2003), particularly that comprising the benthos, leading to a loss of biodiversity, biomass, and the ability to support ecosystem services in estuarine and shelf systems from both social and economic aspects (Diaz & Rosenberg, 1995; Vaquer-Sunyer & Duarte, 2008). Additionally, it contributes to phosphate and iron release (Elrod et al., 2004; Ingall & Jahnke, 1994) and the accumulation of greenhouse gases, including methane, nitrous oxide, and carbon dioxide (D. W. Li et al., 2019; Naqvi et al., 2010).

Journal of Geophysical Research: Oceans 10.1029/2024JC021299

Lu Shou, Hua Lin, Yanyi Miao, Qianwen Sun, Zhibing Jiang, Qicheng Meng, Jiangning Zeng, Feng Zhou, Wei-Jun Cai

Coastal hypoxia develops due to the complex interaction of factors, such as anthropogenic nutrient input from rivers and watersheds, water column stratification, and water and sediment respiration in estuaries and shelf waters (Dai et al., 2023; Fennel & Testa, 2019; Pitcher et al., 2021; Rabalais et al., 2003; Scully, 2010; B. Wang et al., 2017). In general, a necessary condition for the development of coastal hypoxia is enough organic matter that consumes DO in both the water column and sediment. Hypoxia develops if the oxygen consumption rate exceeds the oxygen supply from the atmosphere, nearby waters, and photosynthesizing organisms. Besides the anthropogenic nutrient input, global warming significantly affects coastal hypoxia by enhancing stratification and reducing oxygen solubility (Feng et al., 2012; Meier et al., 2011; Murphy et al., 2011; Scully, 2010).

An increase in flood frequency with uneven regional distributions was predicted to occur due to global warming in East Asia (Hirabayashi et al., 2013; S. Zhang et al., 2022). Floods also significantly influence coastal systems by loading extreme freshwater flux and large amounts of terrestrial matter. The outflow of fresh water mixes with estuarine water, typically forming a river plume, especially for large rivers (Gan et al., 2009; H. Wu et al., 2011). The dynamics of large river plumes are important for coastal biogeochemical processes (Cao et al., 2011; Gong et al., 2011). In 1993, the Mississippi River flood significantly increased nutrient concentrations, biomass, and stratification strength over the Gulf of Mexico shelf, expanding the hypoxic area (Rabalais et al., 1998). The complex interplay between hydrographic and biogeochemical processes triggered by floods likely enhanced hypoxia in the northern Gulf of Mexico (Rabalais et al., 1998). However, whether this mechanism can also be applied to other coastal systems remains unclear, and challenging to determine.

Over the past two decades, the East China Sea shelf has experienced severe hypoxia events, with an even larger hypoxic volume than that in the Gulf of Mexico (Fennel & Testa, 2019; Pitcher et al., 2021; B. Wang et al., 2017; Q. X. Wei et al., 2017; W. X. Zhang et al., 2022). Flooding promotes biomass accumulation over the broad East China Sea shelf (Gong et al., 2011). However, on the inner shelf, the tremendous sediment load during flooding potentially inhibited organic matter production (Ning et al., 1988). Thus, whether hypoxia is exacerbated on the inner shelf during flood periods is unknown. In addition, the Kuroshio waters feed into the bottom waters of the Changjiang Estuary (Hsueh et al., 1992; Zhou et al., 2015), creating a much shorter bottom water residence time than that in the Gulf of Mexico (Fennel & Testa, 2019; Rabouille et al., 2008). The dynamic and complex interactions of these factors make the East China Sea inner shelf an interesting setting for documenting and examining the effects of floods on hypoxia.

In 2020, a historical riverine flood event occurred in the Changjiang catchment of China. We conducted a cruise in the late summer of 2020, to investigate the influence of this historical flooding event on hypoxia on the East China Sea inner shelf. Additionally, the synthesis of biogeochemical data during the flood and non-flood periods was examined to validate the role of flooding in hypoxia development on the shelf.

2. Method

2.1. Samplings and Data Analysis

We conducted a cruise onboard R/V Runjiang I, from 17 to 30 August 2020. Six cross-shelf sections on the East China Sea inner shelf were surveyed from 17 to 22 August (Leg 1, Figure 1a). 18 stations were revisited from 28 to 30 August in the aftermath of Typhoon Bavi (Leg 2, Figure 1a). Heavy rainfall occurred in the Changjiang Basin of China from June to July 2020 (Figure 1b), resulting in an extreme monthly average Changjiang water flux in July, which was ∼1.5 the average flux that had occurred over the past two decades (Figures 1c and 1d).

Water samples were collected using Niskin bottles mounted on a Rosette sampling assembly equipped with a conductivity-temperature-depth recorder (Sea-Bird SBE911). The DO samples were measured using Winkler's method. Subsamples of dissolved inorganic carbon (DIC) were transferred to 350 mL borosilicate bottles and treated with 0.1 mL $HgCl_2$ for storage. The DIC was measured in triplicate using an Apollo Sci-Tec AS-C3 (LI-COR 7000) (Cai et al., 2004; Huang et al., 2012). The precisions of DIC analyses were ±2 μmol kg^{-1}. Certified Reference Materials (CRM) from A. G. Dickson were used for calibration.

Chlorophyll *a* (Chl *a*) and particulate organic carbon (POC) samples were filtered using Whatman GF/F fiber filters (0.7 μm) and stored at −20°C. Dissolved inorganic nutrient samples were filtered using 0.45 μm cellulose acetate filters and frozen to be stored for laboratory analyses. Chl *a* was extracted from the samples with 10 mL of 90% acetone and measured using a Trilogy Laboratory Fluorometer (Turner Designs). To assess POC, samples were dried and weighed to measure total sediment matter (TSM). They were then treated with 2 N HCl to remove

Version of Record at: https://doi.org/10.1029/2024JC021299

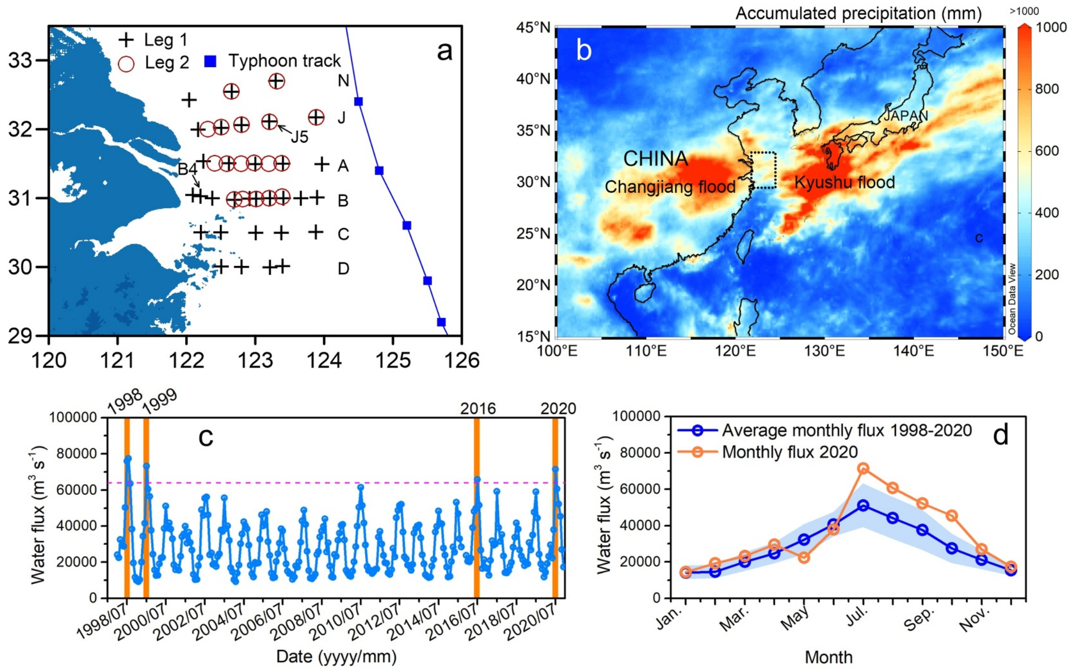

Figure 1. Sampling site of the study and hydrological background of the cruise. (a) Sampling sites of Leg 1 and Leg 2. The trajectory of Typhoon Bavi (2020) was also denoted. (b) Accumulated rainfall (mm) from 1 June to 20 July over East Asia and the Western Pacific Ocean. (c) Monthly Changjiang water flux (m^3 s^{-1}) from 1998 to 2020. (d) Average monthly Changjiang water flux (m^3 s^{-1}). The river flux data were obtained from the Changjiang Maritime Safety Administration (https://cj.msa.gov.cn/).

the particulate inorganic carbon. POC concentrations were determined using an elemental analyzer (Elementa, Germany). The concentrations of nitrate and phosphate were measured with an Auto Discrete Chemical Analyzer (Smartchem 600, AMS Alliance, Italy) in the laboratory using colorimetric methods, as described by Grasshoff et al. (2009).

The apparent oxygen utilization (AOU) was calculated as the difference between the saturated and measured oxygen. The accumulated precipitation data were obtained from the climate prediction center merged analysis of precipitation.

The flood period in this study is defined as the period of the flood event, characterized by the Changjiang water gauge attaining a height of 14.4 m (measured at the Datong hydrological station), per the flood numbering criteria (Ministry of Water Resources of China, 2019). This gauge corresponds to a water flux of about 63,000 m^3 s^{-1} at the Datong hydrological station. Consequently, within the context of this study, the category "flood year" denotes a year featuring at least one such flood event. It should be noted that the effects of flood waters on biogeochemical cycles in the Changjiang Estuary last for weeks to months after the discharge.

The hypoxia area denotes the spatial coverage of waters with DO less than 63 μmol L^{-1}. The DO data were processed using the Kriging interpolation method. And hypoxia area was estimated with Surfer (Golden Software). Temporal fluctuations in the hypoxia area within the Changjiang Estuary were observed throughout the year. For our study, which centers on assessing hypoxia severity in the Changjiang Estuary during a specific year, the maximum observed hypoxia area among different cruises or legs is considered representative of that year's hypoxia extent. The upper boundary depth of hypoxic waters was calculated using linear interpolation. The thickness of hypoxic waters is the difference between the upper boundary depth and station depth. The volume of hypoxic water was obtained by multiplying the hypoxia area by its thickness.

Hypoxia data from multiple years were obtained from our field observations, open data banks, and publications. These are listed in Table 1. The river flux data are obtained from the Changjiang Maritime Safety Administration (https://cj.msa.gov.cn/). The spatial probabilities of hypoxia and high-Chl *a* (>5 μg L^{-1}) plume waters were determined by calculating the ratio of total event occurrences to the total number of years within a specific zone.

Version of Record at: https://doi.org/10.1029/2024JC021299

Table 1
List of Data Sources

Parameters	Method	Sampling date (Year/Month)	Category	Data source
DO	Winkler method	1998/08	Flood year	B. D. Wang (2009)
DO	Seabird CTD	1999/08	Flood year	D. J. Li et al. (2002)
DO	YSI 6600	2003/09	Non-flood year	H. Wei et al. (2007)
DO	Winkler method	2006/08	Non-flood year	Zhu et al. (2011)
DO	Seabird CTD	2008/08, 2009/08	Non-flood year	Liu et al. (2012)
DO	Seabird CTD	2011/08, 2013/08, 2014/08, 2017/08	Non-flood year	Yang et al. (2023)
DO	Winkler method	2016/07	Flood year	Ge et al. (2021)
DO	Winkler method	2016/08	Flood year	J. F. Chen et al. (2020)
DO	Winkler method	2020/08	Flood year	This study
Chl *a*	Chl *a* fluorometer	1998/07	Flood year	Gong et al. (2006)
Chl *a*	Chl *a* fluorometer	2003/08	Non-flood year	Gong et al. (2006)
Chl *a*	Chl *a* fluorometer	2004/07	Non-flood year	Gong et al. (2006)
Chl *a*	Chl *a* fluorometer	2006/07	Non-flood year	K. Wang et al. (2014)
Chl *a*	Chl *a* fluorometer	2011/07	Non-flood year	Tseng et al. (2013)
Chl *a*	Chl *a* fluorometer	2013–2015 July, 2017–2018 July	Non-flood year	W. Q. Li (2022)
Chl *a*	Chl *a* fluorometer	2016/07	Flood year	Ge et al. (2021)
Chl *a*,	Chl *a* fluorometer	2020/08	Flood year	This study

This calculation was performed at a resolution of 0.2° × 0.2° to provide detailed spatial insights into the distribution of hypoxia and high-Chl *a* plume events.

Previous research usually used a salinity criterion of 31 when assessing the coverage of the Changjiang plume. It is the accumulation and falling of organic matter that contributes to hypoxia. And Chl *a* peaked at a salinity of approximately 24 (W. Q. Li et al., 2021). Thus, in this study, we use isohaline of 24 to compare the extension of plume waters. A quantification of high-Chl *a* plume area was defined as the waters with Chl *a* larger than 5 μg L^{-1}.

2.2. End-Member Analysis

To obtain the DIC and DO changes due to biological factors in deep waters (deeper than 20 m), we removed the influence of water parcel mixing using a simple end-member mixing model (B. Wang et al., 2017; H. J. Wang et al., 2016). The end-member mixing model was constructed based on the formulas as follows:

$$f_1 + f_2 + f_3 = 1 \tag{1}$$

$$\theta_1 f_1 + \theta_2 f_2 + \theta_3 f_3 = \theta \tag{2}$$

$$s_1 f_1 + s_2 f_2 + s_3 f_3 = S \tag{3}$$

where f_1, f_2, and f_3 are the fractions of the three end-members, respectively; θ_1, θ_2, and θ_3 are the potential temperature of the three end-members, respectively; s_1, s_2, and s_3 are the salinity of the end-members, respectively; θ and S are the potential temperature and salinity of the samples, respectively.

The nutrient concentration due to the conservative mixing of the three end-members (N_{mix}) and the biological part (N_{bio}) can be calculated as follows:

$$N_1 f_1 + N_2 f_2 + N_3 f_3 = N_{\text{mix}} \tag{4}$$

$$N_{\text{bio}} = N - N_{\text{mix}} \tag{5}$$

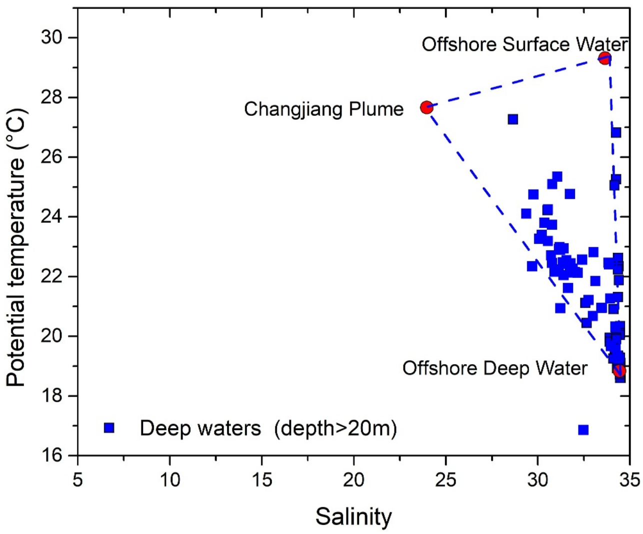

Figure 2. Potential temperature-salinity relationship in the inner shelf in 2020. The end-members are shown with red dots.

where N_1, N_2, and N_3 are the nutrient concentrations of the three end-members, respectively. N is the concentration of the specific water sample.

The estuarine waters are the mixing products of three major water masses: Changjiang Plume Water, warm and saline Offshore Surface Water, and cold Offshore Deep Water, as indicated by the potential temperature-salinity (*T*-*S*) plot (Figure 2). The end-members had also been previously described (B. Wang et al., 2017; K. Wang et al., 2014).

The end-member values are shown in Table 2. The end-member values were obtained by averaging the corresponding water samples. In our model, the Changjiang Plume Water is characterized by heavily reduced DIC, while moderately supersaturated oxygen, a condition that is mediated by air-sea exchange and biological activity (Table 2) (Zhai et al., 2013). We first estimated the water parcel fractions of a water sample. The influence of physical mixing was removed by subtracting the estimated conservative mixing value from the observed value (B. Wang et al., 2017). The outcome denotes the part that results from biological processes. Solar heating will influence sea surface temperature, which produces uncertainties in model results. Thus, we only ran the model for waters deeper than 20 m, well below the thermocline.

3. Results

3.1. Distributions of Surface and Bottom Parameters

In 2020, our cruise revealed extended river plume waters on the East China Sea inner shelf during Leg 1 with high surface nitrate and Chl *a* concentration (maximum of 29.62 μg L^{-1}) (Figures 3a, 3c, and 3d). The hypoxia area (<63 μmol L^{-1}) and low bottom DO (<90 μmol L^{-1}) area covered ∼2,400 and ∼20,300 km^2, respectively (Figure 3i).

Approximately a week later in Leg 2 (28–30 August), we observed more severe hypoxia, covering an area of ∼11,600 km^2, with a minimum DO of 21 μmol L^{-1} (Figure 3m). Moreover, the eastern edge of the hypoxic waters extended eastward to 123.6°E, which was less reported before (W. X. Zhang et al., 2019). The DO in hypoxic waters decreased from 67 to 42 μmol L^{-1} within ∼10 days, which corresponds to an oxygen decrease rate of 2.5 μmol L^{-1} d^{-1}, which represented the net competing balance of biological oxygen consumption and physical oxygen supply.

In Leg 2, bottom water DIC did not increase compared with that in Leg 1 in hypoxic waters (Figures 3j and 3n). The maximum bottom water DIC was 2,163 μmol kg^{-1} in Leg 2 (123.1997°E, 30.9553°N, Figure 3n), which was only close to that in Leg 1 (2,164 μmol kg^{-1}, Figure 3j). The maximum bottom phosphate in Leg 2 decreased from 1.23 to 0.85 μmol L^{-1} in Leg 1 (Figures 3l and 3p).

3.2. Vertical Distributions of Hydrological and Biogeochemical Parameters

Distributions of salinity, temperature, and density all show strong vertical differences from surface to bottom (Figure 4). In Leg 1, the bottom waters in transect B were cold (<19°C) and high in salinity (>34, Figures 4j and 4k). While they were warmer (>20°C) and mild in salinity (<33.5) in transect J (Figures 4b and 4c). In Leg 2, the bottom salinity decreased and temperature increased when compared with that in Leg 1 (Figures 4f, 4g, 4n, and 4o).

Table 2
The End-Member Values of Water Parcels

End-member	Temperature (°C)	Salinity (PSU)	Phosphate (μmol L^{-1})	Nitrate (μmol L^{-1})	DIC (μmol kg^{-1})	DO (μmol kg^{-1})
Changjiang Plume Water	27.68 ± 1.57	23.88 ± 4.90	0.05 ± 0.16	15.17 ± 8.94	1812 ± 135	290 ± 62
Offshore Surface Water	29.32 ± 0.56	33.23 ± 0.48	0.13 ± 0.03	0.48 ± 0.19	1,960 ± 28	212 ± 9
Offshore Deep Water	18.87 ± 0.36	34.46 ± 0.01	0.70 ± 0.03	9.60 ± 0.05	2,092 ± 4	143 ± 6

AGU ADVANCING EARTH AND SPACE SCIENCES
Journal of Geophysical Research: Oceans
10.1029/2024JC021299

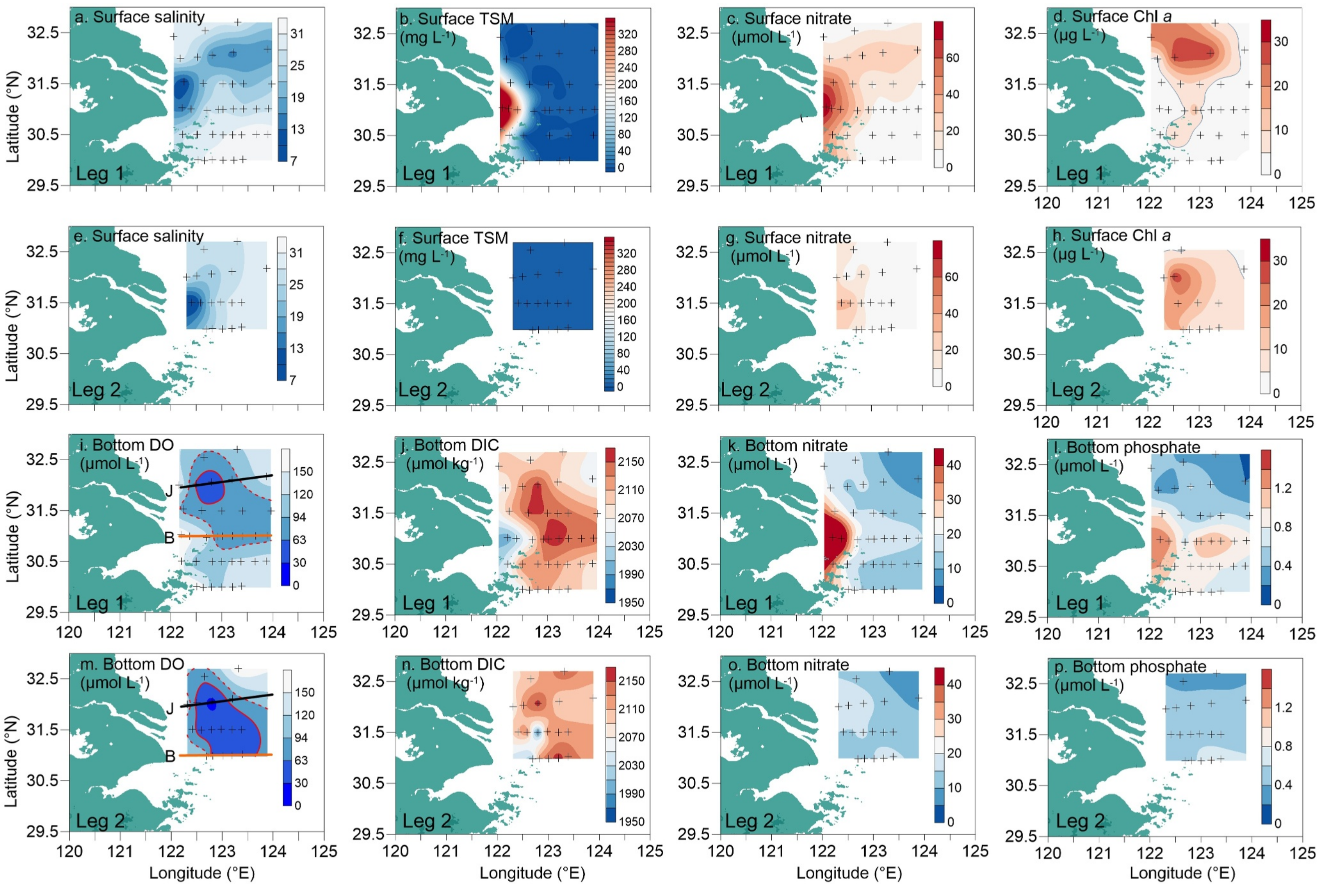

Figure 3. Surface and bottom distributions of parameters in 2020. Surface distributions in Leg 1 and Leg 2 are shown in panels (a–h). Panels (i–p) show bottom distributions. In panels (i and m), the covered red and dashed lines denote the 63 and 96 μmol L^{-1} contour lines, respectively. The black and orange lines mark transects J and B in Figure 4, respectively.

Hypoxic waters with high DIC were observed from a depth of approximately 20 m to the bottom in transect J (Figures 5a, 5b, 5i, and 5j). Surface DO in both transects decreased from Leg 1 to Leg 2. The DO of waters at 20 m in transect B was similar between Leg 1 and Leg 2. While they decrease by about 30 μmol L^{-1} from 30 m to the bottom (Figures 5i and 5m). The average DIC (30 m to bottom) in transect B in Leg 1 and Leg 2 were 2,154 and 2,135 μmol kg^{-1}, respectively. The average phosphate (30 m to bottom) in transect B also decreased by 0.43 μmol L^{-1} from Leg 1 to Leg 2 (Figures 5l and 5p).

4. Discussion

4.1. Extended Flood Plume Waters With High Biological Carbon Production in 2020

The Changjiang River outflow mixes with the estuarine waters, forming the expansive Changjiang plume waters, which extend hundreds of kilometers offshore (Gong et al., 2011). Consequently, the high nutrient load carried by the Changjiang facilitates elevated primary production over a broad coverage, especially in 2020. The August nitrate flux of Changjiang is 1.5 times that of non-flood year (Sun et al., 2023). In August 2020, high nitrate and high-Chl *a* (>5 μg L^{-1}) patch was observed in the surface low-salinity plume waters (Figures 3a and 3d). We observed Chl *a* of 29.62 μg L^{-1} and POC of 868 μg L^{-1} within the high-Chl *a* patch (Table 3), indicating significant organic matter production during the flood. Such high POC was almost twice that observed by Hung et al. (2013) in the Changjiang plume waters. Flooding has also been frequently observed to increase biological carbon production in other river-dominated shelf waters (Ye et al., 2017).

Strong biological productions were also inferred from the relationships between salinity and nutrient, DIC (Figures 6a and 6b). Mixing diagrams are frequently used to validate biological activities. The salinity-nitrate

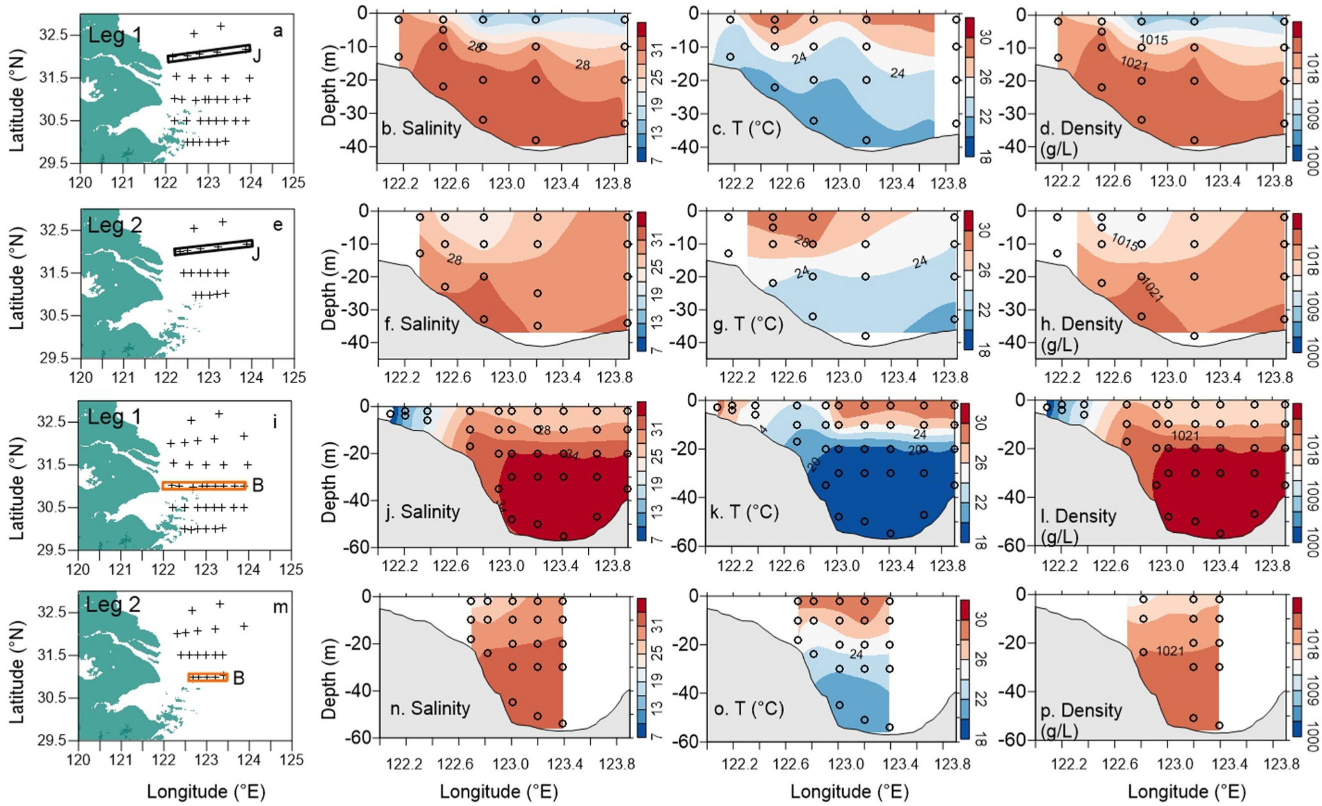

Figure 4. Vertical sections of salinity, temperature (T), and density anomaly during Leg 1 and Leg 2. Section distributions of transect J during Leg 1 and Leg 2 are shown in panels (b–d) and (f–h), respectively. Panels (j–l) and (n–p) show section distributions of transect B during Leg 1 and Leg 2, respectively.

relationship of surface waters (Figure 6a) showed non-conservative mixing within the salinity range of 10–31, which validated the intense biological production, similar to that reported in the Mississippi River plume (Lohrenz et al., 1999). The nitrate consumption due to biological consumption could be up to ~32 μmol L^{-1} if we simply compared the measured value with the conservative two-endmember mixing result (Figure 6a). Biological production was also inferred from the salinity–DIC relationship (Figure 6b), which showed considerable DIC removals along salinity gradients. The minimum DIC during Leg 1 was 1,615 μmol kg^{-1}, observed at a salinity of ~16. The DIC consumption attributed to biological consumption in surface waters across the B, A, N, and J transects during Leg 1 could be estimated to be ~340 μmol kg^{-1} (a spatially-weighted average of 194 ± 130 μmol kg^{-1}), using the method proposed by Xiong et al. (2019) (Figure 6b). In comparison, Xiong et al. (2019) reported an average biologically induced DIC consumption of 211 ± 102 μmol kg^{-1} in the river plume during flooding in July 2016.

During Leg 2, nitrate uptake was also considerable, similar to that observed during Leg 1 (Figure 6a). However, the DIC consumption at a low salinity of ~14 was modest. Conversely, at salinity higher than 23, the biological DIC consumptions were comparable to those observed during Leg 1. Overall, during Leg 2, we also observed significant biological carbon and nitrate consumption, albeit generally lower than that during Leg 1. It's worth noting that Leg 2 was conducted three days after the passage of typhoon Bavi. The biological signals were likely diluted due to typhoon-induced water mixing. Previous research has reported strong biological production triggered by typhoon-induced vertical mixing (D. W. Li et al., 2019). However, it usually occurs approximately a week after the typhoon. Nevertheless, the organic matter produced during and before Leg 1 accumulated in the water column and probably settled to the bottom during Leg 2.

The salinity–Chl a relationship showed double peak values at a salinity of ~16 and ~24 (Figure 6d). Previous research showed Chl a peaked at a salinity of ~28 in the Changjiang Estuary and adjacent shelf (Ning et al., 1988). Light limitation restricts primary production in turbid coastal waters (Ning et al., 1988). And waters with a salinity of ~16 typically stay in the turbid inner estuary during the non-flood periods. In the inner estuary in 2020, the

Journal of Geophysical Research: Oceans 10.1029/2024JC021299

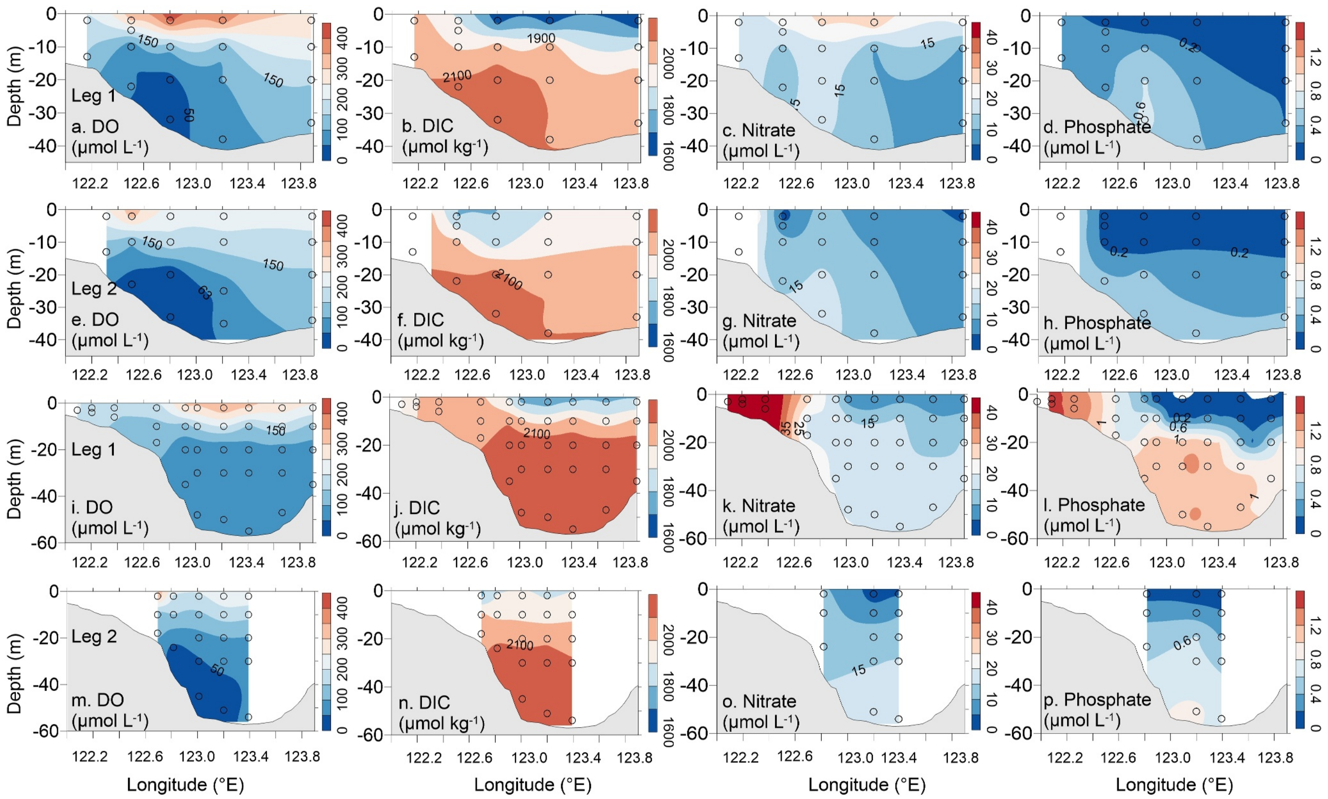

Figure 5. Vertical sections of DO, dissolved inorganic carbon, nitrate, and phosphate during Leg 1 and Leg 2. Section distributions of parameters in transect J during Legs 1 and 2 are shown in panels (a–d) and (e–h), respectively. Panels (i–l) and (m–p) show section distributions of parameters in transect B during Legs 1 and 2, respectively.

maximum TSM concentration was larger than 300 mg L^{-1} (Figure 3b, Table 3). It is expected that Chl *a* was relatively low in the turbid waters (Figure 3d, Table 3).

However, the scatter plot of salinity and Chl *a* of multiple cruises indicated that high-Chl *a* water (>5 μg L^{-1}) had a wide salinity range of 10–32 (Figure 6d) during the flood period of 2020 and 2016. The TSM isoline of 50 μg L^{-1} is located west of 122.5°E (Figure 3b). It seems that suspended particles did not move further offshore when the TSM in 2020 was compared with that in previous non-flood years (Tseng et al., 2013). Though the relationship between TSM and the euphotic zone depth is complex, low TSM generally represents good light conditions (Devlin et al., 2008). Furthermore, the high-nutrient low-salinity waters extended further eastward during the flood period. Thus, phytoplankton in waters at a salinity range of 10–20 can also have favorable light and nutrient conditions (Figure S2 in Supporting Information S1 and Figure 6a).

The expansion of plume waters with high nutrients and light availability implied elevated total organic matter production within the euphotic zone, even if the carbon production rate or concentration did not show a significantly higher value. In 2010 and 1998, the total Chl *a* and carbon fixed in the plume waters tripled due to the larger plume area, despite the primary production rate being lower than that of non-flood periods (Gong et al., 2011). Similarly, the biological signal of a single station did not show a significantly high value, as inferred from our study: the DIC removal during 2020 did not exhibit much larger values compared to the previously

Table 3
Particulate Organic Carbon and Other Parameters of Surface Waters During Leg 1

Station	Longitude (°)	Latitude (°)	Salinity	Temperature (°C)	Chl *a* (μg L^{-1})	POC (μg L^{-1})	TSM (mg L^{-1})
High-Chl *a* patch (J5)	123.203°E	32.111°N	15.33	28.57	29.62	868	5.90
Inner estuary (B4)	122.204°E	31.025°N	13.97	26.51	2.73	2,170	326.60

Journal of Geophysical Research: Oceans 10.1029/2024JC021299

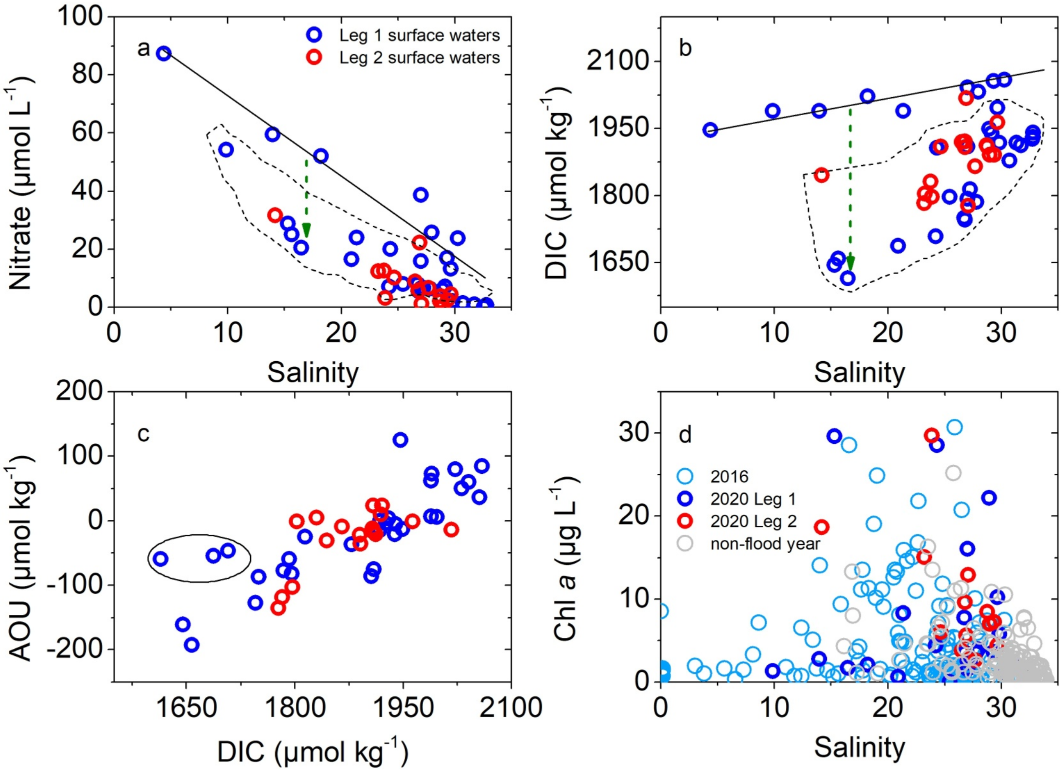

Figure 6. Relationship between various biogeochemical properties of the surface waters (a–d) in 2020. Lines in (a–b) represent the conservative mixing result of low-salinity estuarine waters and oceanic waters. The samples influenced by non-conservative mixing are shown in the dash group. In panel (d), the 2016 data were from Ge et al. (2021), the non-flood periods (2013, 2017, 2018) data were from J. Zhang et al. (2022), Q. S. Wei et al. (2021), and Liblik et al. (2020) In panel (c), apparent oxygen utilization are presented in unit of μmol kg^{-1}, which is approximately 0.98 times that in unit of μmol L^{-1}.

reported value (Xiong et al., 2019). The observed high Chl *a* of 29.62 μg L^{-1} has also been documented in past cruises (Ge et al., 2021; W. Q. Li, 2022; Tseng et al., 2013). Nevertheless, the large high-Chl *a* area indicates an ample supply of organic matter for respiration in the bottom layer.

4.2. Hypoxia During Flood Periods in 2020

The DO value in 2020 was close to the minimum reported in the dynamic East China Sea shelf (B. Wang et al., 2017; H. J. Wang et al., 2016; Q. X. Wei et al., 2017; Zhu et al., 2017). The average thickness of hypoxic waters is approximately 16.4 m during Leg 2. The hypoxia volume was estimated to be 190×10^9 m^3, which was higher than that previously reported from the Gulf of Mexico (92×10^9 m^3) (Fennel & Testa, 2019).

The timing and severity of hypoxic events are determined by the balance of the major oxygen sink and source terms (Fennel & Testa, 2019). The onset of severe hypoxia during a flood period is triggered by an enhanced oxygen sink, a reduced oxygen supply, or both. Flooding events may enhance the development of hypoxia through the strong surface production and subsequent respirations of organic matter at the bottom. As discussed, the surface high Chl *a* concentration and significant nitrate removal reveal strong organic matter production during flood periods in 2020.

The bottom DIC in hypoxic waters was 2,164 μmol kg^{-1}, much higher than the DIC from the background DIC value (~2,070 μmol kg^{-1}) (B. Wang et al., 2017; Xiong et al., 2020). Such DIC addition can only be achieved by the decomposition of organic matter. The decomposition of organic matter can also be revealed by determining the relationship between DO, DIC, and nutrients (Zhu et al., 2011). Significant relationships of DIC–AOU, and nitrate–phosphate for the deep waters (below thermocline, no less than 20 m) during Leg 1 and Leg 2 were observed (Figures 7a and 7b, $p < 0.01$). The regression slope of the AOU and DIC (1.053) in the southern deep waters of Leg 1 was generally in agreement with the Redfield ratio (O: C = 138:106), which is the stoichiometry

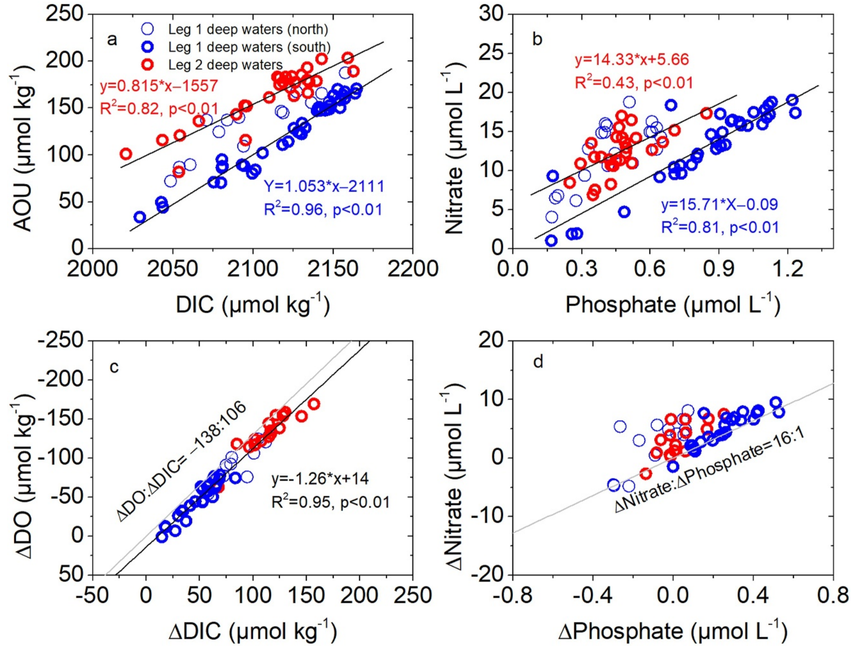

Figure 7. Relationships between various biogeochemical properties of the deep waters in 2020. Black lines in (a–b) denote the regression line. Gray lines in (c–d) show the lines of the Redfield ratio. In panels (a and c), apparent oxygen utilization and ΔDO are presented in units of μmol kg^{-1}, which is approximately 0.98 times that in μmol L^{-1}.

of marine phytoplankton organic matter decomposition, indicating the effects of organic matter respiration. Such relationships between biogenic elements have also been observed in hypoxic waters in other systems (Xue et al., 2015; Zhai et al., 2015; Zhao et al., 2020).

The hypoxia area exhibits significant temporal variations, as inferred from the results of Leg 1 (~2,400 m^2) and Leg 2 (11,600 m^2) of our study in 2020. The bottom distribution of DO and DIC showed a decrease of DO and DIC in waters from Leg 1 to Leg 2 (Figures 3i, 3j, 3m, and 3n), which was inconsistent with the effects of organic matter decomposition. Wind patterns modulate the hypoxia except for the organic matter decomposition triggered by riverine nutrient input. Leg 2 of our study was conducted 3 days following the passage of Typhoon Bavi, positioned approximately 50 km east of the easternmost station. Intense wind event is associated with vertical mixing, disrupting stratification, and increasing bottom DO (Ni et al., 2016).

A comparison of density profiles between Leg 1 and Leg 2 showed the persistence of stratification, suggesting the typhoon did not thoroughly mix the water column. While the bottom density and salinity decreased in the deep waters of transect B in Leg 2 compared with that in Leg 1 (Figures 4l and 4p). Also, the phosphate concentrations were generally lower than that in Leg 1 (Figures 3l and 3p), suggesting that the bottom waters were influenced by low-salinity and low-phosphate plume waters (Ni et al., 2016). The passing typhoon Bavi (22 August) could deepen the mixed lay depth, similar to the typhoon's influences in the western North Pacific Ocean (Q. Y. Wu & Chen, 2012).

The signal of mixing or diffusion of surface waters into waters below the thermocline can also be seen in the DIC–AOU relationship. The regression results of DIC–AOU for the deep-water samples in Leg 2 differed from those in Leg 1. Surface water DO equilibrates with the atmosphere in about a week, while it takes a much longer time, perhaps several months, to equilibrate the mix-layer CO_2 (Zeebe & Wolf-Gladrow, 2001). Thus, the surface waters probably have nearly equilibrated DO but unsaturated CO_2 (Zhai et al., 2013). Such a scenario was supported by the observations of reduced DIC but moderate AOU in surface waters during Leg 1 (Figure 6c, oval). The CO_2-reduced but nearly oxygen-equilibrated surface waters could influence the AOU–DIC ratio in shallow stations, by vertical advection or mixing during typhoon Bavi. Previous research also observed different excess DIC–AOU relationships between shallow stations and deep stations in the northern East China Sea, resulting from different equilibrium times of DO and carbon in surface waters (Xiong et al., 2020). To justify our hypothesis, we constructed an end-member mixing, which is described in the Method.

Our model results show that the estimated biologically induced DIC (ΔDIC) and DO (ΔDO) changes were significantly related in the deep waters in the two Legs (Figure 7c, $p < 0.01$). Additionally, this ratio agreed with the canonical Redfield ratio, which confirmed that DO depletion was dominated by community respiration (Xiong et al., 2020). The change in nitrate (ΔN) and phosphate (ΔP) roughly followed the Redfield ratio (N:P = 16:1), which was consistent with the inference regarding marine-origin organic matter decomposition (Figure 7d).

The diffusion or mixing of oxygen-rich surface waters by Typhoon Bavi introduces oxygen to the bottom waters, which causes the opposite effect on the increase in the hypoxia area from Leg 1 to Leg 2. During Leg 1 of 2020, we observed a large plume with high nutrient and high Chl *a* (>5 μmol L^{-1}). The abundant organic matter accumulated and respirated in the bottom from Leg 1 to Leg 2. Besides, a substantial area with low DO (<90 μM) was observed in Leg 1 (20,300 km^2). Considering the time scale for hypoxia development in the Changjiang Estuary spans days to weeks (Ni et al., 2016; B. Wang et al., 2017), the significant increase in hypoxia area from Leg 1 to Leg 2 (2,400 to 11,600 km^2) was reasonable. A previous study suggested that typhoon-induced currents could transport the hypoxic waters offshore (Meng, Zhou, et al., 2022), thereby expanding the hypoxia area. If the high-phosphate bottom waters from the west advect offshore (Figures 5i and 5p), the bottom phosphate should have increased from Leg 1 to Leg 2. However, the decrease in bottom phosphate indicated a limited influence of advection. In summary, the biological decomposition of accumulated organic matter leads to severe hypoxia.

The ΔDIC and ΔDO in transect B (20 m to bottom, average depth of 33 m) increase by approximately 41 and 50 μmol kg^{-1} from Leg 1 to Leg 2, respectively. The net respiration rate can be estimated as 41 (μmol C kg^{-1})/10 d × 33 m × 1,021 (kg m^{-3}) × 12 (g mol^{-1}) = 1.66 g m^{-2} d^{-1}, which is higher than the estimation of B. Wang et al. (2017). Both observed oxygen decreasing rate (2.5 μmol L^{-1} d^{-1}) and the estimated ΔDO increasing rate (5.0 μmol kg^{-1} d^{-1}) are higher than the apparent DO depletion rate (1.8 μmol kg^{-1} d^{-1}) (Xiong et al., 2020), suggesting enhanced respiration during the flood period. Previous research also inferred strong respiration during flood periods. The community respiration rate within the euphotic zone was higher during the flood years in the East China Sea (C.-C. Chen et al., 2017). In an estuary in the western Gulf of Mexico, floods also elevate community respiration and drive the system to net heterotrophic (Bruesewitz et al., 2013). In the semi-closed North Yellow Sea, strong net community respiration leads to low $CaCO_3$ saturation states after a summer flood (Zhai et al., 2015).

Generally, the respiration signals can be either from the water column or from the sediment-water interface. In the Changjiang Estuary, major oxygen sink was attributed to biological oxygen consumption in the water column, fueled by freshly produced organic matter (B. Wang et al., 2017; H. J. Wang et al., 2016). A comprehensive analysis indicated a hypoxic thickness-dependent sediment contribution (Fennel & Testa, 2019). The thickness of hypoxic waters in transect B is ∼33 m. The depth-integrated ΔDO increasing rate can be estimated as 50 (μmol O_2 kg^{-1})/10 d × 33 m × 1,021 (kg m^{-3}) = 168 mmol O_2 m^{-2} d^{-1}. Previous sediment oxygen consumption rates obtained using batch incubation revealed the average and maximum rates of 8.4 and 17.6 mmol O_2 m^{-2} d^{-1}, respectively, in the East China Sea (Song et al., 2016). This maximum rate represented only 10.4% of the observed biological oxygen consumption rate in the column. Results from a pelagic-benthic coupled model also supported the importance of oxygen sinks in water columns (Meng, Zhang, et al., 2022). The contribution of sediment oxygen loss can be substantial in shallow hypoxic water, such as the northern Gulf of Mexico (Rowe et al., 2002).

Besides the fresh autochthonous organic matter, the decomposition of terrestrial materials can also enhance oxygen sinks in coastal waters (Swarzenski et al., 2008). Floods contribute to hypoxia by promoting the respiration of floodplain vegetation and sewage in estuaries (Wong et al., 2010). In the East China Sea inner shelf, terrestrial particles were typically confined to a narrow area on the inner estuary, as indicated by a sharp decrease in the TSM (Figure 3b). Hypoxic waters were located northeast of the estuary (Figure 3i). Therefore, the contribution of terrestrial matter to hypoxia was limited per our results. The high Chl *a* in the plume waters also indicated a source of fresh oceanic organic matter in the plume waters, concurring with that reported by B. Wang et al. (2017).

The total supply of fresh organic matter is primarily constrained by nutrient inputs within the euphotic zone (Lohrenz et al., 1999; K. Wang et al., 2014), especially riverine nutrients. The nutrient input from flood waters determines the potential for biological organic matter production under favorable light conditions. Large plume areas with abundant organic matter during the flood period favored the hypoxia development in the East China Sea inner shelf, which was similar to the hypoxia development in the northern Gulf of Mexico during the flood

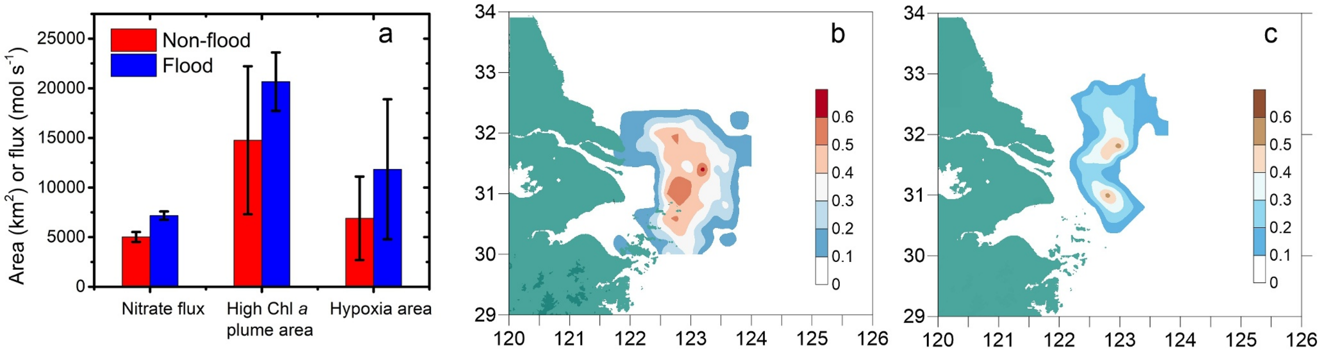

Figure 8. Variations in Changjiang nitrate flux, high-Chl *a* plume area (>5 μg L^{-1}), and hypoxic area during non-flood and flood periods (a). Probability of high Chl *a* (>5 μg L^{-1}) occurrence (b) and probability of hypoxia occurrence (c). Data were cited from published literature (J. F. Chen et al., 2020; Ge et al., 2021; Gong et al., 2006; D. J. Li et al., 2002; W. Q. Li, 2022; Liu et al., 2012; Tseng et al., 2013; B. D. Wang, 2009; K. Wang et al., 2014; H. Wei et al., 2007; Yang et al., 2023; Zhu et al., 2011) and our study. The data sources are listed in Table 1 and the estimated method is shown in the Method section.

period in 1993 (Rabalais et al., 1998). While typhoons influence hypoxia by vertical mixing and horizontal advection as a short-term event, determining their net contribution to hypoxia, and quantitatively differentiating their role from that of flood in hypoxia development poses challenges.

4.3. Hypoxia During Flood and Non-Flood Years

To validate the influences of flood on surface biological production of plume waters and hypoxia on the inner shelf, we collected DO, Chl *a,* and other biogeochemical data during both the non-flood and flood years. The data sources are listed in Table 1. During the flood years (1998, 1999, 2016, and 2020), the average riverine nitrate flux was approximately 1.4 times that of the non-flood years (Figure 8a). The spatial distributions of isohaline and nitrate isoline in 1998, 2016, and 2020 showed an eastward extension of high-nutrient plume waters (Figures 9a and 9b). The high-nutrient plume waters during the flood periods covered much larger areas than those in the other normal-flux periods. The plume dynamics in estuaries are influenced by various factors, including river flux, topography, tide, wind patterns, and regional currents (Liu et al., 2021; Schiller et al., 2011). Previous studies in the Changjiang Estuary and other estuarine systems have indicated that large river flux during flooding periods enlarge the river plume area (Gong et al., 2011; Rabalais et al., 1998).

No significant difference in turbidity front was observed between the flood and non-flood periods (Figure 9c), probably because the massive particles carried by the floods settled rapidly (J. Li & Zhang, 1998; Liblik et al., 2020). The turbidity front was calculated based on the method of W. Q. Li et al. (2021). In the inner shelf, plume waters with high biological production rates are usually located within a narrow belt between the turbidity and plume fronts (W. Q. Li et al., 2021), with sufficient nutrients and light. During the flood period, the belt with replete nutrients and favorable light conditions extended when compared with those during the non-flood periods (Figure 9).

Multiple-year observations also revealed a much larger patch of high-Chl *a* (defined as >5 μg L^{-1}) plume waters during the flood year (Figure 8a). It agrees with previous flood research on the broad East China Sea shelf and the Gulf of Mexico (Gong et al., 2011; Rabalais et al., 1998). Chl *a* is typically used to assess biological carbon production, although the ratio of Chl *a* and carbon varies across systems and scenarios (Chang et al., 2003; Jakobsen & Markager, 2016). Generally, a larger high-Chl *a* area indicates elevated total organic matter production. Bottom organic matter accumulation links surface organic matter production and hypoxia in the bottom waters. However, the bottom organic carbon data are too scarce to reveal differences between flood year and non-flood year. Additionally, bottom organic carbon is heavily influenced by the sediment suspension process (Hung et al., 2013). Notwithstanding, Deng et al. (2006) proposed that less than 20% of carbon inventory over the shelf is buried, with the majority of POC produced being decomposed. Thus, the additional supply of organic matter in upper waters probably contributes to hypoxia development. Our historical data showed that the average hypoxic area during the flood years (11,400 ± 7,000 km^2) was about 1.7 times that during the non-flood years (6,900 ± 4,200 km^2) (Figure 8a). The flood exerts its influences by spreading plume waters, which are nutrient-replete, and biologically active.

Journal of Geophysical Research: Oceans 10.1029/2024JC021299

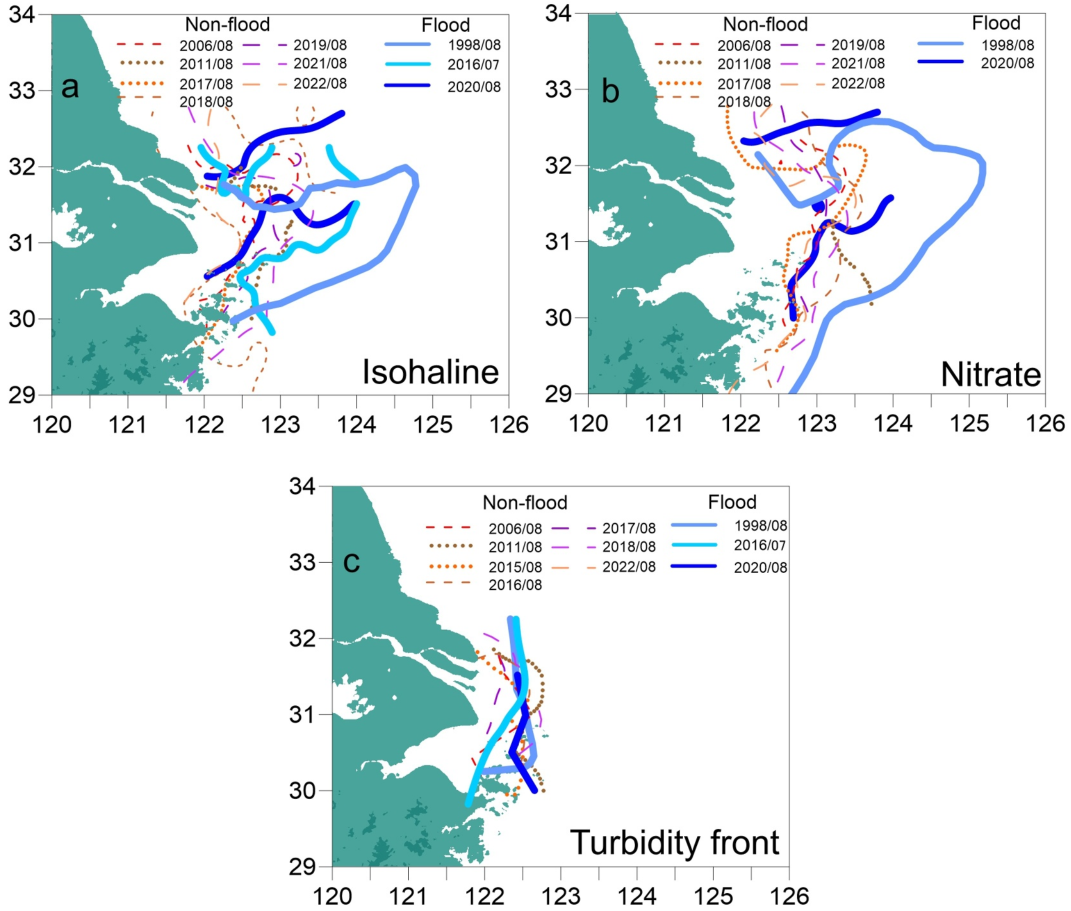

Figure 9. Variations in (a) isohaline of 24; (b) nitrate contour line of 10 μmol L^{-1}; (c) turbidity front during non-flood and flood years. Data from 1998 to 2015 were cited from published literature (Gao et al., 1999; Ge et al., 2021; Tseng et al., 2013; B.-D. Wang et al., 2003; K. Wang et al., 2014), Data from 2017 to 2022 were collected by this study.

The significance of plume waters in influencing bottom hypoxia was underscored by the spatial distribution of the probability of hypoxia and high-Chl *a* plume water (>5 μg L^{-1}), which revealed a spatial correlation between high-Chl *a* plume waters and hypoxic hotspot on the inner shelf (Figures 8b and 8c). Compilation of multiple surveys in the Gulf of Mexico also showed that the highest frequency of hypoxia occurrence located down current from the discharges of the Mississippi and Atchafalaya Rivers (Rabalais et al., 2003), aligning with the direction of river plume movement. This implied that as Chl *a* and biologically-produced organic matter extend offshore with plume waters, the hypoxic area may expand.

In summary, during a flood, massive nitrate discharge is carried eastward by plume waters. The area of plume waters with high nutrient and light availability expands compared to non-flood years. Consequently, total carbon production in the upper layer increases, leading to greater organic carbon accumulation at the bottom. The respiration of this elevated bottom organic matter results in severe hypoxia during flood periods.

Initially, nutrients fuel surface biological production. A nutrient-based linear regression method has been proposed to predict hypoxia area in the northern Gulf of Mexico (Donner & Scavia, 2007). In the inner shelf of the East China Sea, the relationship between riverine nitrate flux and hypoxia area is "scatter" (Figure S3 in Supporting Information S1). This scatter relationship is largely due to wind disturbances, particularly from typhoons, which can substantially modulate hypoxia areas in summer. Previous research has documented a notable increase in DO following wind events in the Changjiang Estuary (Ni et al., 2016). Similarly, in the Gulf of Mexico, wind influences hypoxia areas by shifting plume water and altering stratification (Feng et al., 2012). Additionally, the fluctuating intrusion of the Taiwan Warm Current Bottom varies annually, impacting hypoxia areas through the advection of low-oxygen waters.

Both the average hypoxia water area and high-Chl *a* area exhibit large standard errors, demonstrating the dynamic nature of the inner shelf (Figure 8a). During the flood years 1999, 2016, and 2020, the hypoxic areas exceeded 10,000 km^2. Gong et al. (2011) reported that the total Chl *a* (in tons) and carbon fixed (in tons carbon per day) in plume waters in July 1998 were about three times that during the non-flood years. However, the observed hypoxic area was much smaller, only about ~600 km^2 in 1998. In addition to physical factors such as wind disturbances and offshore water advection, the observed limited hypoxia area in 1998 can also be attributed to the timing of observations. Previous studies have suggested a decoupling of surface Chl *a* and bottom hypoxia in the Changjiang Estuary, likely due to the time delay between surface production and bottom respiration in such a dynamic system (Zhou et al., 2020). The single-cruise observation conducted from July 24 to August 17 may have missed the peak hypoxic area, which is typically observed in late August in the East China Sea (D. J. Li et al., 2002; B. Wang et al., 2017; H. J. Wang et al., 2016; Zhu et al., 2017).

5. Conclusion

In summary, our study documented a severe bottom hypoxia event during the flood period in 2020, characterized by a maximum hypoxia area estimated at ~11,600 km^2, and a minimum DO concentration of 21 μmol L^{-1}. Significant biological nitrate and DIC uptake, and high Chl *a* in surface waters indicate intense organic matter production. Furthermore, the decomposition of organic matter in deep waters consumes DO, leading to hypoxia.

Riverine floods were found to be associated with the expansion of the high-nutrient plume area during the flood periods, while turbid waters remained confined to the inner estuary. The expansion of river plume waters, rich in high nutrients, led to an expansion of the high-Chl *a* area. This expansion significantly increased the hypoxia area when compared to non-flood years.

Data Availability Statement

The field-measured data in 2020 were collected on a cruise jointly funded by the National Programme on Global Change and Air-Sea Interaction (Phase II)—Hypoxia and Acidification Monitoring and Warning Project in the Changjiang Estuary, and the Long Term Observation and Research Plan in the Changjiang Estuary and the Adjacent East China Sea Project of the Second Institute of Oceanography, MNR. These data have been published in the Mendeley Data (https://doi.org/10.17632/drrdbshf2f.2) (D. W. Li et al., 2024).

Acknowledgments
We thank the crews of the Runjiang I and the colleagues on the cruise for their support in sample collections. We are grateful to Ying Luo and Chen Zeng for POC sample analysis and data collection. This research was jointly supported by National Programme on Global Change and Air-Sea Interaction (Phase II)—Hypoxia and Acidification Monitoring and Warning Project in the Changjiang Estuary, Scientific Research Fund of the Second Institute of Oceanography, MNR (QNYC2203), National Natural Science Foundation of China (No. 42276046; 41806095), Science Foundation of Donghai Laboratory (Grants DH-2022KF0201, DH-2022ZY0006), Zhejiang Provincial Natural Science Foundation of China (LD24D060001). We thank the anonymous reviewers for their insightful suggestions on improving the manuscript.

References

Breitburg, D., Levin, L. A., Oschlies, A., Grégoire, M., Chavez, F. P., Conley, D. J., et al. (2018). Declining oxygen in the global ocean and coastal waters. *Science*, *359*(6371), eaam7240. https://doi.org/10.1126/science.aam7240

Bruesewitz, D. A., Gardner, W. S., Mooney, R. F., Pollard, L., & Buskey, E. J. (2013). Estuarine ecosystem function response to flood and drought in a shallow, semiarid estuary: Nitrogen cycling and ecosystem metabolism. *Limnology and Oceanography*, *58*(6), 2293–2309. https://doi.org/10.4319/lo.2013.58.6.2293

Cai, W.-J., Dai, M. H., Wang, Y. C., Zhai, W. D., Huang, T., Chen, S. T., et al. (2004). The biogeochemistry of inorganic carbon and nutrients in the Pearl River estuary and the adjacent Northern South China Sea. *Continental Shelf Research*, *24*(12), 1301–1319. https://doi.org/10.1016/j.csr.2004.04.005

Cao, Z. M., Dai, M. H., Zheng, N., Wang, D. L., Li, Q., Zhai, W. D., et al. (2011). Dynamics of the carbonate system in a large continental shelf system under the influence of both a river plume and coastal upwelling. *Journal of Geophysical Research*, *116*(G2), G02010. https://doi.org/10.1029/2010JG001596

Chang, J., Shiah, F.-K., Gong, G.-C., & Chiang, K. P. (2003). Cross-shelf variation in carbon to chlorophyll *a* ratios in the East China Sea, summer 1998. *Deep Sea Research Part II: Topical Studies in Oceanography*, *50*(6), 1237–1247. https://doi.org/10.1016/s0967-0645(03)00020-1

Chen, C.-C., Gong, G.-C., Chou, W.-C., Chung, C.-C., Hsieh, C.-H., Shiah, F.-K., & Chiang, K.-P. (2017). The influence of episodic flooding on a pelagic ecosystem in the East China Sea. *Biogeosciences*, *14*(10), 2597–2609. https://doi.org/10.5194/bg-14-2597-2017

Chen, J. F., Li, D. W., Jin, H., Jiang, Z., Wang, B., Wu, B., et al. (2020). Changing nutrients, oxygen and phytoplankton in the East China Sea. In C.-T. A. Chen & X. Guo (Eds.), *Changing Asia-Pacific Marginal Seas* (pp. 155–178). Springer Singapore. https://doi.org/10.1007/978-981-15-4886-4_10

Dai, M. H., Zhao, Y., Chai, F., Chen, M., Chen, N., Chen, Y., et al. (2023). Persistent eutrophication and hypoxia in the coastal ocean. *Cambridge Prisms: Coastal Futures*, *1*, e19. https://doi.org/10.1017/cft.2023.7

Deng, B., Zhang, J., & Wu, Y. (2006). Recent sediment accumulation and carbon burial in the East China Sea. *Global Biogeochemical Cycles*, *20*(3), GB3014. https://doi.org/10.1029/2005gb002559

Devlin, M., Barry, J., Mills, D., Gowen, R., Foden, J., Sivyer, D., & Tett, P. (2008). Relationships between suspended particulate material, light attenuation and Secchi depth in UK marine waters. *Estuarine, Coastal and Shelf Science*, *79*(3), 429–439. https://doi.org/10.1016/j.ecss.2008.04.024

Diaz, R. J., & Rosenberg, R. (1995). Marine benthic hypoxia, a review of its ecological effects and the behavioural responses of benthic macrofauna. *Oceanography and Marine Biology*, *33*, 245–303.

Donner, S. D., & Scavia, D. (2007). How climate controls the flux of nitrogen by the Mississippi River and the development of hypoxia in the Gulf of Mexico. *Limnology and Oceanography*, *52*(2), 856–861. https://doi.org/10.4319/lo.2007.52.2.0856

Elrod, V. A., Berelson, W. M., Coale, K. H., & Johnson, K. S. (2004). The flux of iron from continental shelf sediments: A missing source for global budgets. *Geophysical Research Letters*, *31*(12), L12307. https://doi.org/10.1029/2004GL020216

Feng, Y., Dimarco, S. F., & Jackson, G. A. (2012). Relative role of wind forcing and riverine nutrient input on the extent of hypoxia in the northern Gulf of Mexico. *Geophysical Research Letters*, *39*(9), L09601. https://doi.org/10.1029/2012gl051192

Fennel, K., & Testa, J. M. (2019). Biogeochemical controls on coastal hypoxia. *Annual Review of Marine Science*, *11*(1), 105–130. https://doi.org/10.1146/annurev-marine-010318-095138

Gan, J. P., Li, L., Wang, D. X., & Guo, X. (2009). Interaction of a river plume with coastal upwelling in the northeastern South China Sea. *Continental Shelf Research*, *29*(4), 728–740. https://doi.org/10.1016/j.csr.2008.12.002

Gao, S., Cheng, P., Wang, Y., & Cao, Q. (1999). Characteristics of suspended sediment concentrations over the area adjacent to the Changjiang River Estuary, the summer of 1998 (in Chinese with English abstract). *Marine Science Bulletin*, *18*(6), 44–50.

Ge, J. Z., Zhang, J., Chen, C., & Ding, P. (2021). Impacts of fluvial flood on physical and biogeochemical environments in estuary–shelf continuum in the East China Sea. *Journal of Hydrology*, *598*, 126441. https://doi.org/10.1016/j.jhydrol.2021.126441

Gong, G. C., Chang, J., Chiang, K., Hsiung, T., Hung, C., Duan, S., & Codispoti, L. A. (2006). Reduction of primary production and changing of nutrient ratio in the East China Sea: Effect of the Three Gorges Dam? *Geophysical Research Letters*, *33*(7), L07610. https://doi.org/10.1029/2006gl025800

Gong, G. C., Liu, K. K., Chiang, K. P., Hsiung, T. M., Chang, J., Chen, C. C., et al. (2011). Yangtze River floods enhance coastal ocean phytoplankton biomass and potential fish production. *Geophysical Research Letters*, *38*(13), L13603. https://doi.org/10.1029/2011GL047519

Grasshoff, K., Kremling, K., & Ehrhardt, M. (2009). *Methods of seawater analysis*. John Wiley & Sons.

Hirabayashi, Y., Mahendran, R., Koirala, S., Konoshima, L., Yamazaki, D., Watanabe, S., et al. (2013). Global flood risk under climate change. *Nature Climate Change*, *3*(9), 816–821. https://doi.org/10.1038/nclimate1911

Hsueh, Y., Wang, J., & Chern, C. S. (1992). The intrusion of the Kuroshio across the continental shelf northeast of Taiwan. *Journal of Geophysical Research*, *97*(C9), 14323–14330. https://doi.org/10.1029/92jc01401

Huang, W. J., Wang, Y. C., & Cai, W.-J. (2012). Assessment of sample storage techniques for total alkalinity and dissolved inorganic carbon in seawater: Sample storage techniques for TA and DIC. *Limnology and Oceanography: Methods*, *10*(9), 711–717. https://doi.org/10.4319/lom.2012.10.711

Hung, C. C., Tseng, C. W., Gong, G. C., Chen, K. S., Chen, M. H., & Hsu, S. C. (2013). Fluxes of particulate organic carbon in the East China Sea in summer. *Biogeosciences*, *10*(10), 6469–6484. https://doi.org/10.5194/bg-10-6469-2013

Ingall, E., & Jahnke, R. (1994). Evidence for enhanced phosphorus regeneration from marine sediments overlain by oxygen depleted waters. *Geochimica et Cosmochimica Acta*, *58*(11), 2571–2575. https://doi.org/10.1016/0016-7037(94)90033-7

Ito, T., Minobe, S., Long, M. C., & Deutsch, C. (2017). Upper ocean O_2 trends: 1958–2015. *Geophysical Research Letters*, *44*(9), 4214–4223. https://doi.org/10.1002/2017GL073613

Jakobsen, H. H., & Markager, S. (2016). Carbon-to-chlorophyll ratio for phytoplankton in temperate coastal waters: Seasonal patterns and relationship to nutrients. *Limnology and Oceanography*, *61*(5), 1853–1868. https://doi.org/10.1002/lno.10338

Li, D. J., Zhang, J., Huang, D. J., Wu, Y., & Liang, J. (2002). Oxygen depletion off the Changjiang (Yangtze River) estuary. *Science in China - Series D: Earth Sciences*, *45*(12), 1137–1146. https://doi.org/10.1360/02yd9110

Li, D. W., Chen, J. F., Ni, X. B., Wang, K., Zeng, D. Y., Wang, B., et al. (2019). Hypoxic bottom waters as a carbon source to atmosphere during a typhoon passage over the East China Sea. *Geophysical Research Letters*, *46*(20), 11329–11337. https://doi.org/10.1029/2019gl083933

Li, D. W., Chen, J. F., Wang, B., Jin, H. Y., Shou, L., Miao, Y. Y., et al. (2024). Hypoxia observations in the East China Sea inner shelf in 2020 [Dataset]. *Mendeley Data, V2*. https://doi.org/10.17632/drrdbshf2f.2

Li, J., & Zhang, C. (1998). Sediment resuspension and implications for turbidity maximum in the Changjiang Estuary. *Marine Geology*, *148*(3–4), 117–124. https://doi.org/10.1016/s0025-3227(98)00003-6

Li, W. Q. (2022). *Dynamic response of spatio-temporal variation of Chl* a *concentration to the fronts in the Changjiang Estuary* (in Chinese) (p. 152). East China Normal University.

Li, W. Q., Ge, J. Z., Ding, P. X., Ma, J. F., Glibert, P. M., & Liu, D. Y. (2021). Effects of dual fronts on the spatial pattern of chlorophyll-a concentrations in and off the Changjiang River Estuary. *Estuaries and Coasts*, *44*(5), 1408–1418. https://doi.org/10.1007/s12237-020-00893-z

Liblik, T., Wu, Y. J., Fan, D. D., & Shang, D. H. (2020). Wind-driven stratification patterns and dissolved oxygen depletion off the Changjiang (Yangtze) Estuary. *Biogeosciences*, *17*(10), 2875–2895. https://doi.org/10.5194/bg-17-2875-2020

Liu, Z., Gan, J., Wu, H., Hu, J., Cai, Z., & Deng, Y. (2021). Advances on coastal and estuarine circulations around the Changjiang Estuary in the recent decades (2000–2020). *Frontiers in Marine Science*, *8*, 615929. https://doi.org/10.3389/fmars.2021.615929

Liu, Z., Xu, R., Liu, C., Qin, Y., & Cai, P. (2012). Characters of hypoxia area off the Yangtze River Estuary and its influence (in Chinese with English abstract). *Marine Science Bulletin*, *31*(5), 588–593.

Lohrenz, S. E., Fahnenstiel, G. L., Redalje, D. G., Lang, G. A., Dagg, M. J., Whitledge, T. E., & Dortch, Q. (1999). Nutrients, irradiance, and mixing as factors regulating primary production in coastal waters impacted by the Mississippi River plume. *Continental Shelf Research*, *19*(9), 1113–1141. https://doi.org/10.1016/s0278-4343(99)00012-6

Meier, H. E. M., Andersson, H. C., Eilola, K., Gustafsson, B. G., Kuznetsov, I., Müller-Karulis, B., et al. (2011). Hypoxia in future climates: A model ensemble study for the Baltic Sea. *Geophysical Research Letters*, *38*(24), L24608. https://doi.org/10.1029/2011GL049929

Meng, Q. C., Zhang, W. Y, Zhou, F., Liao, Y. B., Yu, P. S., Tang, Y. B., et al. (2022). Water oxygen consumption rather than sediment oxygen consumption drives the variation of hypoxia on the East China Sea Shelf. *Journal of Geophysical Research: Biogeosciences*, *127*(2), e2021JG006705. https://doi.org/10.1029/2021JG006705

Meng, Q. C., Zhou, F., Ma, X., Xuan, J. L., Zhang, H., Wang, S., et al. (2022). Response process of coastal hypoxia to a passing typhoon in the East China Sea. *Frontiers in Marine Science*, *9*. https://doi.org/10.3389/fmars.2022.892797

Ministry of Water Resources of China. (2019). Flood numbering regulations for major rivers across the country.

Murphy, R. R., Kemp, W. M., & Ball, W. P. (2011). Long-term trends in Chesapeake Bay seasonal hypoxia, stratification, and nutrient loading. *Estuaries and Coasts*, *34*(6), 1293–1309. https://doi.org/10.1007/s12237-011-9413-7

Naqvi, S., Bange, H. W., Farías, L., Monteiro, P., Scranton, M., & Zhang, J. (2010). Marine hypoxia/anoxia as a source of CH_4 and N_2O. *Biogeosciences*, *7*(7), 2159–2190. https://doi.org/10.5194/bg-7-2159-2010

Ni, X. B., Huang, D. J., Zeng, D. Y., Zhang, T., Li, H. L., & Chen, J. (2016). The impact of wind mixing on the variation of bottom dissolved oxygen off the Changjiang Estuary during summer. *Journal of Marine Systems*, *154*, 122–130. https://doi.org/10.1016/j.jmarsys.2014.11.010

Ning, X. R., Vaulot, D., Liu, Z., & Liu, Z. (1988). Standing stock and production of phytoplankton in the estuary of the Changjiang (Yangtze River) and the adjacent East China Sea. *Marine Ecology Progress Series*, *49*, 141–150. https://doi.org/10.3354/meps049141

Pitcher, G. C., Aguirre-Velarde, A., Breitburg, D., Cardich, J., Carstensen, J., Conley, D. J., et al. (2021). System controls of coastal and open ocean oxygen depletion. *Progress in Oceanography*, *197*, 102613. https://doi.org/10.1016/j.pocean.2021.102613

Rabalais, N. N., Turner, R. E., Wiseman, J., William, J., & Dortch, Q. (1998). Consequences of the 1993 Mississippi River flood in the Gulf of Mexico. *Regulated Rivers: Research & Management: An International Journal Devoted to River Research and Management*, *14*(2), 161–177. https://doi.org/10.1002/(sici)1099-1646(199803/04)14:2<161::aid-rrr495>3.0.co;2-j

Rabalais, N. N., Turner, R. E., & Wiseman, J. W. (2003). Gulf of Mexico hypoxia, A.K.A. "The dead zone". *Annual Review of Ecology, Evolution, and Systematics*, *33*(1), 235–263. https://doi.org/10.1146/annurev.ecolsys.33.010802.150513

Rabouille, C., Conley, D., Dai, M., Cai, W.-J., Chen, C., Lansard, B., et al. (2008). Comparison of hypoxia among four river-dominated ocean margins: The Changjiang (Yangtze), Mississippi, Pearl, and Rhone rivers. *Continental Shelf Research*, *28*(12), 1527–1537. https://doi.org/10.1016/j.csr.2008.01.020

Rowe, G. T., Kaegi, M. E. C., Morse, J. W., Boland, G. S., & Escobar Briones, E. G. (2002). Sediment community metabolism associated with continental shelf hypoxia, northern Gulf of Mexico. *Estuaries*, *25*(6), 1097–1106. https://doi.org/10.1007/bf02692207

Schiller, R., Kourafalou, V., Hogan, P., & Walker, N. (2011). The dynamics of the Mississippi River plume: Impact of topography, wind and offshore forcing on the fate of plume waters. *Journal of Geophysical Research*, *116*(C6), C06029. https://doi.org/10.1029/2010jc006883

Scully, M. E. (2010). The importance of climate variability to wind-driven modulation of hypoxia in Chesapeake Bay. *Journal of Physical Oceanography*, *40*(6), 1435–1440. https://doi.org/10.1175/2010jpo4321.1

Song, G. D., Liu, S. M., Zhu, Z. Y., Zhai, W. D., Zhu, C. J., & Zhang, J. (2016). Sediment oxygen consumption and benthic organic carbon mineralization on the continental shelves of the East China Sea and the Yellow Sea. *Deep Sea Research Part II: Topical Studies in Oceanography*, *124*, 53–63. https://doi.org/10.1016/j.dsr2.2015.04.012

Sun, Q. W., Li, D. W., Wang, B., Xu, Z. S., Miao, Y. Y., Lin, H., et al. (2023). Massive nutrients offshore transport off the Changjiang Estuary in flooding summer of 2020. *Frontiers in Marine Science*, *10*, 97. https://doi.org/10.3389/fmars.2023.1076336

Swarzenski, P., Campbell, P., Osterman, L., & Poore, R. (2008). A 1000-year sediment record of recurring hypoxia off the Mississippi River: The potential role of terrestrially-derived organic matter inputs. *Marine Chemistry*, *109*(1–2), 130–142. https://doi.org/10.1016/j.marchem.2008.01.003

Tseng, Y.-F., Lin, J., Dai, M. H., & Kao, S.-J. (2013). Joint effect of freshwater plume and coastal upwelling on phytoplankton growth off the Changjiang River. *Biogeosciences*, *10*(6), 10363–10397.

Vaquer-Sunyer, R., & Duarte, C. M. (2008). Thresholds of hypoxia for marine biodiversity. *Proceedings of the National Academy of Sciences*, *105*(40), 15452–15457. https://doi.org/10.1073/pnas.0803833105

Wang, B., Chen, J. F., Jin, H. Y., Li, H. L, Huang, D. J., & Cai, W.-J. (2017). Diatom bloom-derived bottom water hypoxia off the Changjiang estuary, with and without typhoon influence. *Limnology and Oceanography*, *62*(4), 1552–1569. https://doi.org/10.1002/lno.10517

Wang, B. D. (2009). Hydromorphological mechanisms leading to hypoxia off the Changjiang estuary. *Marine Environmental Research*, *67*(1), 53–58. https://doi.org/10.1016/j.marenvres.2008.11.001

Wang, B.-D., Wang, X.-L., & Zhan, R. (2003). Nutrient conditions in the Yellow Sea and the East China Sea. *Estuarine, Coastal and Shelf Science*, *58*(1), 127–136. https://doi.org/10.1016/s0272-7714(03)00067-2

Wang, H. J., Dai, M. H., Liu, J., Kao, S.-J., Zhang, C., Cai, W.-J., et al. (2016). Eutrophication-driven hypoxia in the East China Sea off the Changjiang Estuary. *Environmental Science and Technology*, *50*(5), 2255–2263. https://doi.org/10.1021/acs.est.5b06211

Wang, K., Chen, J. F., Jin, H. Y., Li, H. L., Gao, S. Q., Xu, J., et al. (2014). Summer nutrient dynamics and biological carbon uptake rate in the Changjiang River plume inferred using a three end-member mixing model. *Continental Shelf Research*, *91*, 192–200. https://doi.org/10.1016/j.csr.2014.09.013

Wei, H., He, Y., Li, Q., Liu, Z., & Wang, H. (2007). Summer hypoxia adjacent to the Changjiang Estuary. *Journal of Marine Systems*, *67*(3–4), 292–303. https://doi.org/10.1016/j.jmarsys.2006.04.014

Wei, Q. S., Yao, P., Xu, B. C., Zhao, B., Ran, X. B., Zhao, Y. H., et al. (2021). Coastal upwelling combined with the river plume regulates hypoxia in the Changjiang Estuary and adjacent inner East China Sea shelf. *Journal of Geophysical Research: Oceans*, *126*(11), e2021JC017740. https://doi.org/10.1029/2021jc017740

Wei, Q. X., Wang, B. D., Yu, Z. G., Chen, J. F., & Xue, L. (2017). Mechanisms leading to the frequent occurrences of hypoxia and a preliminary analysis of the associated acidification off the Changjiang estuary in summer. *Science China Earth Sciences*, *60*(2), 360–381. https://doi.org/10.1007/s11430-015-5542-8

Wong, V. N. L., Johnston, S. G., Bush, R. T., Sullivan, L. A., Clay, C., Burton, E. D., & Slavich, P. G. (2010). Spatial and temporal changes in estuarine water quality during a post-flood hypoxic event. *Estuarine, Coastal and Shelf Science*, *87*(1), 73–82. https://doi.org/10.1016/j.ecss.2009.12.015

Wu, H., Zhu, J. R., Shen, J., & Wang, H. V. (2011). Tidal modulation on the Changjiang River plume in summer. *Journal of Geophysical Research*, *116*(C8), C08017. https://doi.org/10.1029/2011JC007209

Wu, Q. Y., & Chen, D. K. (2012). Typhoon-induced variability of the oceanic surface mixed layer observed by Argo floats in the western North Pacific Ocean. *Atmosphere-Ocean*, *50*(sup1), 4–14. https://doi.org/10.1080/07055900.2012.712913

Xiong, T. Q., Liu, P. F., Zhai, W. D., Bai, Y., Liu, D., Qi, D., et al. (2019). Export flux, biogeochemical effects, and the fate of a terrestrial carbonate system: From Changjiang (Yangtze River) Estuary to the East China Sea. *Earth and Space Science*, *6*(11), 2115–2141. https://doi.org/10.1029/2019ea000679

Xiong, T.-Q., Wei, Q.-S., Zhai, W.-D., Li, C.-L., Wang, S.-Y., Zhang, Y.-X., et al. (2020). Comparing subsurface seasonal deoxygenation and acidification in the Yellow Sea and northern East China Sea along the north-to-south latitude gradient. *Frontiers in Marine Science*, *7*, 686. https://doi.org/10.3389/fmars.2020.00686

Xue, J. H., Cai, W.-J., Hu, X., Huang, W.-J., Lohrenz, S. E., & Gundersen, K. (2015). Temporal variation and stoichiometric ratios of organic matter remineralization in bottom waters of the northern Gulf of Mexico during late spring and summer. *Journal of Geophysical Research: Oceans*, *120*(12), 8304–8326. https://doi.org/10.1002/2015JC011453

Yang, X. X., Fan, H., Zhang, H., Chen, S., Yang, Y., Ji, H., et al. (2023). Regulation of water masses to hypoxia zones in the Changjiang Estuary. *Journal of Ocean University of China*, *22*(4), 993–1002. https://doi.org/10.1007/s11802-023-5345-7

Ye, F., Guo, W., Shi, Z., Jia, G., & Wei, G. (2017). Seasonal dynamics of particulate organic matter and its response to flooding in the Pearl River Estuary, China, revealed by stable isotope ($\delta_{13}C$ and $\delta^{15}N$) analyses. *Journal of Geophysical Research: Oceans*, *122*(8), 6835–6856. https://doi.org/10.1002/2017JC012931

Zeebe, R. E., & Wolf-Gladrow, D. (2001). *CO_2 in seawater: Equilibrium, kinetics, isotopes* (p. 100). Elsevier Science.

Zhai, W. D., Dai, M. H., Chen, B. S., Guo, X. H., Li, Q., Shang, S. L., et al. (2013). Seasonal variations of sea–air CO_2 fluxes in the largest tropical marginal sea (South China Sea) based on multiple-year underway measurements. *Biogeosciences*, *10*(11), 7775–7791. https://doi.org/10.5194/bg-10-7775-2013

Zhai, W.-D., Zang, K.-P., Huo, C., Zheng, N., & Xu, X.-M. (2015). Occurrence of aragonite corrosive water in the North Yellow Sea, near the Yalu River estuary, during a summer flood. *Estuarine, Coastal and Shelf Science*, *166*, 199–208. https://doi.org/10.1016/j.ecss.2015.02.010

Zhang, J., Zhu, X., Zhang, R., Ren, J., Wu, Y., Liu, S., & Huang, D. (2022). Dissolved Fe in the East China Sea under the influences of land sources and the boundary current with implications for global marginal seas. *Global Biogeochemical Cycles*, *36*(2), e2021GB006946. https://doi.org/10.1029/2021gb006946

Zhang, S., Zhou, L., Zhang, L., Yang, Y., Wei, Z., Zhou, S., et al. (2022). Reconciling disagreement on global river flood changes in a warming climate. *Nature Climate Change*, *12*(12), 1160–1167. https://doi.org/10.1038/s41558-022-01539-7

Zhang, W. X., Dunne, J. P., Wu, H., Zhou, F., & Huang, D. (2022). Using timescales of deficit and residence to evaluate near-bottom dissolved oxygen variation in coastal seas. *Journal of Geophysical Research: Biogeosciences*, *127*(1), e2021JG006408. https://doi.org/10.1029/2021jg006408

Zhang, W. X., Wu, H., Hetland, R. D., & Zhu, Z. (2019). On mechanisms controlling the seasonal hypoxia hot spots off the Changjiang River Estuary. *Journal of Geophysical Research: Oceans*, *124*(12), 8683–8700. https://doi.org/10.1029/2019jc015322

Zhao, Y. Y., Liu, J., Uthaipan, K., Song, X., Xu, Y., He, B., et al. (2020). Dynamics of inorganic carbon and pH in a large subtropical continental shelf system: Interaction between eutrophication, hypoxia, and ocean acidification. *Limnology and Oceanography*, *65*(6), 1359–1379. https://doi.org/10.1002/lno.11393

Zhou, F., Chai, F., Huang, D. J., Wells, M., Ma, X., Meng, Q. C., et al. (2020). Coupling and decoupling of high biomass phytoplankton production and hypoxia in a highly dynamic coastal system: The Changjiang (Yangtze River) Estuary. *Frontiers in Marine Science*, *7*, 259. https://doi.org/10.3389/FMARS.2020.00259

Zhou, F., Xue, H. J., Huang, D. J., Xuan, J. L., Ni, X. B., Xiu, P., & Hao, Q. (2015). Cross-shelf exchange in the shelf of the East China Sea. *Journal of Geophysical Research: Oceans*, *120*(3), 1545–1572. https://doi.org/10.1002/2014jc010567

Zhu, Z.-Y., Wu, H., Liu, S.-M., Wu, Y., Huang, D.-J., Zhang, J., & Zhang, G.-S. (2017). Hypoxia off the Changjiang (Yangtze River) estuary and in the adjacent East China Sea: Quantitative approaches to estimating the tidal impact and nutrient regeneration. *Marine Pollution Bulletin*, *125*(1–2), 103–114. https://doi.org/10.1016/j.marpolbul.2017.07.029

Zhu, Z.-Y., Zhang, J., Wu, Y., Zhang, Y.-Y., Lin, J., & Liu, S.-M. (2011). Hypoxia off the Changjiang (Yangtze River) Estuary: Oxygen depletion and organic matter decomposition. *Marine Chemistry*, *125*(1), 108–116. https://doi.org/10.1016/j.marchem.2011.03.005